Photochemical CO_2 reduction using structurally controlled g-C_3N_4

James J. Walsh,[a] Chaoran Jiang,[b] Junwang Tang[b*] and Alexander J. Cowan[a]*

The published form of the article can be found in Physical Chemistry Chemical Physics, 2016, DOI: 10.1039/C6CP04525A

Graphitic carbon nitride (g-C_3N_4) synthesised from a urea precursor is an excellent CO_2 reduction photocatalyst using $[Co(bpy)_n]^{2+}$ as a co-catalyst. A five-fold increase in activity for the highly polymerised urea derived g-C_3N_4 is achieved compared to alternative precursors. Transient absorption, time-resolved and steady-state emission studies indicate that the enhanced activity is related to both an increased driving force for photoelectron transfer and a greater availability of photogenerated charges.

Increasing atmospheric CO_2 levels due to anthropogenic activity has brought carbon capture and carbon utilisation into the public consciousness and to the forefront of chemical research. The reduction of CO_2 to useful feedstocks or fuels such as CO, formic acid and methanol can be achieved through photochemical, electrochemical and thermal methods. The photochemical reduction of CO_2 is particularly attractive as when coupled to light driven water oxidation it offers a route to carbon based solar fuels. Whilst significant progress has been made in recent years towards the delivery of efficient semiconductor photocatalysts for water oxidation,[1] the development of a visible light active, scalable, stable, photocatalytic system for CO_2 reduction in the presence of water remains an un-realised goal.

g-C_3N_4 is an organic polymeric photocatalyst that has been intensely studied for photocatalytic hydrogen evolution [2, 3, 4, 5 6, 7, 8, 9] and to a lesser extent water oxidation,[3, 10] since a landmark study in 2009.[2] The band gap of g-C_3N_4 (typically *ca*. 2.5 eV) enables visible light activity. In addition, g-C_3N_4 has been shown to be photochemically and mechanically stable and relatively facile to synthesise.[11, 12] In addition a diverse range of approaches towards enhancing the visible light activity of g-C_3N_4 have been reported including g-C_3N_4/metal oxide heterojunctions,[13] dye-sensitised g-C_3N_4 [14] and full photocatalytic water splitting z-schemes.[15] Of particular significance to this study is that some of us have recently shown that platinized g-C_3N_4 prepared from different precursors can have markedly different levels of photocatalytic activity, with a urea-derived material achieving an internal quantum efficiency (IQE) of 26.5 % for hydrogen production, greatly exceeding previously reported g-C_3N_4 photocatalysts.[16] This very high level of photocatalytic activity, an order of magnitude greater than comparable materials prepared from different precursors, was found to correlate to an increased degree of polymerization and decreased proton concentration within the urea based g-C_3N_4.

In contrast to the substantial literature relating to hydrogen evolution there are a more limited number of studies examining the use of g-C_3N_4 for CO_2 reduction in the presence of water.[17, 18, 19 20, 21] One issue is that to overcome competitive proton reduction to H_2 in the presence of water a selective CO_2 reduction co-catalyst is required. Recently Maeda *et al*., have developed a range of $[Ru(bpy)(CO)_2Cl_2]$ derivatives (bpy = 2,2'-bipyridine) where modification of the 4,4' positions of bpy has enabled either direct or indirect binding to g-C_3N_4,[20, 21] giving rise to a material that reduced CO_2 to formate with an apparent quantum yield (AQY) of 5.7% at 400 nm.[22] Alternative approaches have explored the use of scalable co-catalysts on g-C_3N_4 including $[Co(bpy)_n]^{2+}$.[17, 18, 19] In these studies the co-catalyst, which is assembled *in-situ*, has been shown to be effective for CO production with an AQY of 0.25% at 420 nm and excellent selectivity.[18] Whilst these reports clearly demonstrate the potential application of g-C_3N_4 for CO_2 reduction, to date there have been relatively few systematic studies on exploring the nature of the g-C_3N_4 used with each co-catalyst. Herein we examine a range of carbon nitrides, including the previously reported highly active urea derived g-C_3N_4,[16] for CO_2 reduction. The simple *in-situ* prepared $[Co(bpy)_n]^{2+}$ co-catalyst is chosen as it has been reported to be highly effective with a wide range of different light absorbers,[19] making it an ideal test platform to explore the role of different g-C_3N_4 structures derived from a range of precursors. We report both an enhancement in the activity for a g-C_3N_4/$[Co(bpy)_n]^{2+}$ mediated CO_2 reduction system and an improved overall understanding into the factors controlling the high levels of activity of urea derived g-C_3N_4 in reductive photochemistry.

g-C_3N_4 was prepared from three different precursors (urea, thiourea and dicyandiamide (DCDA)) in the manner previously described, see ESI for full details.[16] Previous reports on the g-C_3N_4/$[Co(bpy)_n]^{2+}$ system have demonstrated successful CO_2 reduction in a solvent mixture of CH_3CN/H_2O with triethanolamine (TEOA) also being added as a sacrificial electron donor[17, 18, 19] and the same solvent system is also employed here (CH_3CN:H_2O:TEOA, 3:1:1, 5 ml total). In the presence of urea derived g-C_3N_4 (2.5 mg), $CoCl_2$ (50 μmol dm^{-3}), bpy (5 mmol dm^{-3}) under an atmosphere of CO_2 we observe photocatalytic CO production with minimal H_2 evolution (CO:H_2, 3.3:1), see Table 1. In the absence of any one of these components CO_2 reduction does not occur (Table S1). A brief optimization of the concentrations of the catalyst components is presented in the ESI (Figs. S1, S2); however we highlight that the focus of this study is the optimization and mechanistic study of the g-C_3N_4 absorber. The lack of CO production in the absence of CO_2 and isotopic labelling studies (Fig. S7) definitively confirmed CO_2 to be the carbon source for CO.[18] The lack of CO_2 reduction in the absence of the bipyridine ligand is also in agreement with past electrochemical and photochemical studies of this co-catalyst, which has previously supported an assignment of the active catalyst precursor to a molecular species, proposed to be $[Co(bpy)_n]^{2+}$.[23, 24]

$g\text{-}C_3N_4$ precursor	SSA ($m^2.g^{-1}$)[a]	Band gap (eV)	CO rate $\mu mol.g^{-1}.h^{-1}$ /TON[b]	H_2 rate $\mu mol.g^{-1}.h^{-1}$/TON[b]	Selectivity (CO:H_2)
Urea	43.8	2.9	460/9.2	138/2.8	3.3:1
Thiourea	18.5	2.5	22/0.4	86/1.7	0.25:1
DCDA	12.8	2.6	92/1.8	94/1.9	~ 1:1

Table 1: Photocatalytic activity for CO_2 reduction of the different $g\text{-}C_3N_4$ materials. Experiments carried out using 300 – 795 nm KG1 filter (Fig. S3), 40 $mW.cm^{-2}$ illumination, 0.5 mg $g\text{-}C_3N_4$ per ml in $CH_3CN/TEOA/H_2O$ (3:1:1), t = 2 h. a: Specific surface area, see reference 16; b: TON per Co^{2+} at t = 2 hours.

Under Xe lamp illumination (300 -795 nm) a turnover number (TON) per Co^{2+} of greater than 9 was achieved after 2 hours for CO production using urea derived $g\text{-}C_3N_4$, Table 1. At prolonged periods it was found that the rate of CO_2 production began to decrease. To explore the factors limiting the TON experiments using a 400 nm LED were carried out, Fig. 1 (a). The use of a blue LED with a small spectral distribution allows for excitation of the $g\text{-}C_3N_4$ whilst avoiding the potential photochemical degradation of the reduced $[Co(bpy)_n]^+$ (λ_{max} ~ 600 nm).[24] After 6 hours of illumination at 400 nm the CO yield plateaued with a TON corresponding to *ca.* 10.6. Flushing the flask with fresh CO_2 leads to a recovery of activity and the system was able to achieve a TON > 18 before the experiment was terminated. This recovery in activity may indicate that a build-up of CO inhibits catalysis, either through CO interacting with the $g\text{-}C_3N_4$, or more likely through inhibition of the co-catalyst. It is noted that CO inhibition has been previously reported during CO_2 photoreduction with other Co^{2+} catalysts.[25]

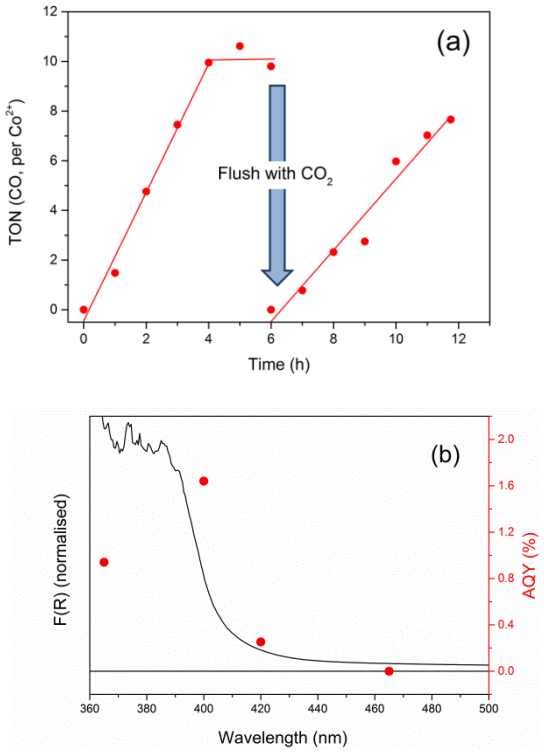

Fig. 1: Photocatalytic CO_2 reduction under (a) prolonged 400 nm LED illumination (ca. 5 $mW.cm^{-2}$). (b) AQY for CO production measured at wavelengths shown (red) and overlaid UV/Vis spectrum of the reaction suspension. Conditions: $g\text{-}C_3N_4$ (urea, 2.5 mg), $CoCl_2$ (50 $\mu mol\ dm^{-3}$) and bpy (5 $mmol\ dm^{-3}$) in 5 ml $CH_3CN:H_2O:TEOA$, 3:1:1 purged with CO_2.

Previous hydrogen evolution studies have found that the photocatalytic activity of platinized urea derived $g\text{-}C_3N_4$ is significantly greater than other precursor materials.[16] Similarly the highest efficiency material for CO_2 reduction using $[Co(bpy)_n]^{2+}$ as a co-catalyst is $g\text{-}C_3N_4$ (urea), with relative catalytic efficiencies following the trend urea > DCDA > thiourea. The CO yield from $g\text{-}C_3N_4$ (urea) was 5x higher than that from DCDA-derived $g\text{-}C_3N_4$, and 23x higher than that from thiourea-derived $g\text{-}C_3N_4$, Table 1. The CO/H_2 selectivity was also 3.3x or 13.3x higher, respectively. Interestingly the relative enhancements in activity for CO_2 reduction reported here are similar to those reported for H_2 production using $g\text{-}C_3N_4$/Pt, where $g\text{-}C_3N_4$ (urea) produces H_2 at a rate of 8x relative to $g\text{-}C_3N_4$ (DCDA) and 13.5x relative to $g\text{-}C_3N_4$ (thiourea).[16] In order to benchmark the activity of the urea derived system for CO_2 reduction we have recorded the AQY, also known as the

photonic efficiency,[26] at a range of wavelengths (Fig. 1 (b)). The AQY response of g-C_3N_4 (urea) and $[Co(bpy)_n]^{2+}$ matches well to the recorded UV/Vis spectrum of g-C_3N_4. Direct comparison of efficiencies between this study and others by AQY is complicated as the AQY does not take into account the number of photons absorbed, only those incident on the sample (see ESI for the calculations). However it is apparent that the activity of the urea g-C_3N_4 is at the same level of greater than current state-of-the-art g-C_3N_4 (melamine)/CoO_x/$[Co(bpy)_n]^{2+}$ systems for CO_2 reduction which utilised a ten-fold more concentrated suspension of g-C_3N_4 to achieve a maximum AQY of 0.25 % at 420 nm and noted only a small increase in activity at 400 nm.[18] In contrast here we reach a maximum AQY of 1.6 % at 400 nm and at 420 nm, a wavelength where incomplete light harvesting occurs in our reactor (Fig. 1 (b)), an AQY 0.25 % is also achieved. The maximum AQY of 1.6 % is indeed comparable to other state of the art CO_2 reduction photocatalysts.[20, 27, 28]

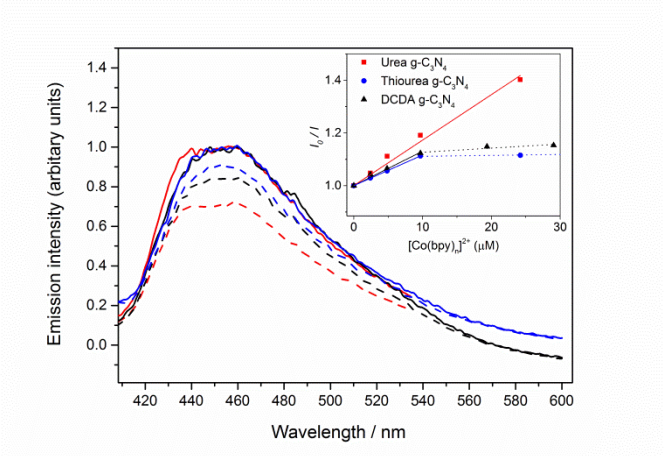

Fig. 2: Normalised emission of urea (red), DCDA (black) and thiourea (blue) derived g-C_3N_4 (0.1 mg ml^{-1} in 1:1 CH_3CN/H_2O) in the absence of a quencher (solid lines) and relative quenching in the presence of $[Co(bpy)_n]^{2+}$ (dashed lines). Inset shows the Stern-Volmer plots for g-C_3N_4 in CH_3CN/H_2O with a $[Co(bpy)_n]^{2+}$ quencher.

It is striking that the relative trends for the activity of urea, DCDA and thiourea derived g-C_3N_4 are the same for both CO_2 reduction and H_2 evolution.[16] This change in activity cannot be attributed to improved light harvesting of the urea derived material as it displays a wider band gap than both the DCDA and thiourea samples (Table 1, Fig. S4). The photocatalytic CO_2 activity also does not scale linearly with the relative BET surface areas of the materials, Table 1. It has been previously noted that the activity for the different materials for hydrogen evolution correlates with the degree of material hydrogenation (i.e.: the ratio of surface sp^2 nitrogen sites (C-N-C) to sp^3 sites (H-N-$[C]_3$ and C-NH_x)).[16] DFT calculations indicated that two possible enhancement routes were occurring in materials with high sp^2:sp^3 ratios. Firstly the observed wider band gap of urea derived g-C_3N_4 leads to a raising of the conduction band edge (Fig. S4), which will increase the driving force for electron transfer to any co-catalyst. Secondly a greater level of exciton delocalization was proposed to occur in g-C_3N_4 (urea), minimizing fast exciton recombination and increasing the yield of separated charges which are required for photocatalysis to occur.[16] Here we have explored the potential role of both effects in the photocatalytic CO_2 reduction system. Photoluminescence (PL) occurs in g-C_3N_4 after bandgap excitation due to electron-hole recombination, displaying maxima ranging from 440 – 460 nm. In the presence of an electron acceptor it is known that this emission can be quenched by electron transfer to $[Co(bpy)_n]^{2+}$.[18] Quenching studies in the absence and presence of $[Co(bpy)_n]^{2+}$ were performed (Fig. 2). A Stern-Volmer (SV) plot shows a good linear response for concentrations of co-catalyst up to 10 μmol dm^{-3}. Notably the slopes of the SV plots yielded K_{SV} constants (Table S2) with values following the sequence urea > DCDA > thiourea, which mirrors the sequence of photocatalytic activity (transient emission studies indicate a similar lifetime for the emissive states in all three materials, Fig. S5), and the driving force for electron transfer calculated by DFT and TD-DFT previously.[16] We also note that for thiourea and DCDA derived g-C_3N_4 no additional quenching occurs at $[Co(bpy)_n]^{2+}$ concentrations above 10 μmol dm^{-3}. The lack of linearity at higher quenching concentrations may indicate a population of inaccessible emissive states.[29] In DCDA and thiourea derived materials it is proposed that a significant population of photogenerated charges are trapped at sites inaccessible to the solution, hence making them photochemically less active. In contrast the urea derived g-C_3N_4 displays reasonable linearity at quencher concentrations up to 24 μmol dm^{-3}, it is apparent therefore that both the increased driving force for electron transfer from the conduction band of urea derived g-C_3N_4 to the $[Co(bpy)_n]^{2+}$ catalyst and the greater accessibility to the g-C_3N_4 surface are important factors behind the enhanced photocatalytic activity of this material.

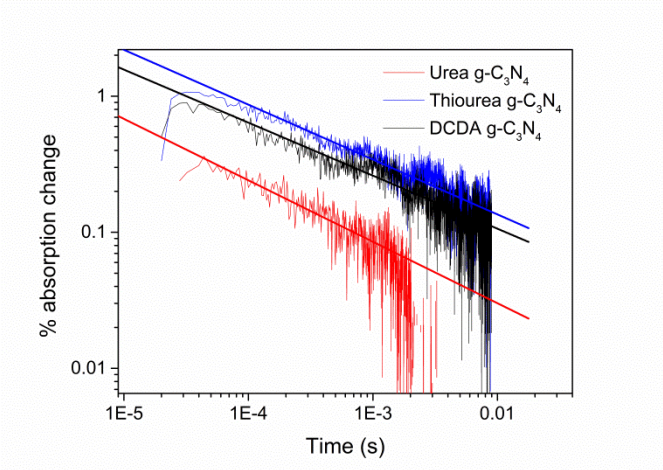

Fig. 3: DR-TA kinetic traces recorded at 850 nm for the g-C_3N_4 sample indicated under an Argon atmosphere, following UV (355 nm, 91 μJ.cm^{-2}) excitation.

Transient absorption (TA) spectroscopy is a powerful tool to probe the change in concentration of charge carriers (photogenerated electrons and holes) with time[30] and here we also examine the diffuse reflectance TA kinetics of the g-C_3N_4 samples. Recently it has been highlighted that long-lived photogenerated charges can persist in g-C_3N_4 into the milliseconds timescales and it has been proposed that these are important in controlling photocatalytic efficiency.[22, 31] Following UV (355 nm, 6 ns pulse, 91 μJ.cm^{-2}) excitation we observe a broad long-lived feature in the visible/NIR region that persists for significantly longer timescales (signals remain at > 10 ms after excitation at 850 nm) than the strong emission that is observed between 400 – 600 nm (lifetime *ca.* 8 ns, Fig. S5). Again a clear trend between the different g-C_3N_4 samples is noted with the urea derived sample having a far lower yield of long-lived TA features when compared to the DCDA and thiourea samples. Full DR-TA spectra of all samples are shown in Fig. S6. In recent studies similar g-C_3N_4 TA features in the visible region have been assigned to trapped electrons or potentially electron-hole pairs and the same assignment is proposed here.[22, 32, 33] The decay kinetics of the TA features at 850 nm are found to fit well to a power law model (%abs $\propto t^{-\beta}$, $\beta = 0.42 \pm 0.05$) for all three g-C_3N_4 samples studied which is likely to indicate that charge recombination is occurring *via* a trap-detrap mechanism, Fig. 3.[34] The weaker long-lived TA signals in our most active photocatalyst is perhaps surprising as it is often suggested that the ability to generate higher yields of long-lived charges is a characteristic of the most active semiconductor photocatalysts.[35] Indeed in a recent study on photoelectrochemical water splitting using a protonated g-C_3N_4 embedded in Nafion such a trend was noted; however it is important to highlight in this case water oxidation was studied and the protonated sample actually had a lower sp^2 N/sp^3 ratio than the untreated g-C_3N_4.[31] In contrast a recent TA study of g-C_3N_4 by Kuriki *et al.*[22] reported the presence of deeply trapped inactive charges in the visible region. Furthermore in the TA experiments presented here, which are carried out under an argon atmosphere in the absence of the water/g-C_3N_4 interface, defect sites may be critical in overcoming the large exciton binding energy[36] of g-C_3N_4 leading to the presence of deeply trapped charges. Therefore, in light of the (i) observed trap-mediated recombination kinetics (ii) the inverse correlation between photocatalytic activity and long-lived charge TA signal and (iii) the previous observation in the emission quenching study of inaccessible sites on DCDA/thiourea g-C_3N_4 we propose that the transient absorption observed here at 850 nm also correlates to deep lying, kinetically less reactive, photogenerated charges. The DCDA and thiourea samples appear to have a higher density of deep lying less photochemically active trap states than the urea derived material which is leading to decreased photocatalytic activity for both CO_2 reduction and hydrogen evolution.

Conclusions

We have tested a family of g-C_3N_4 polymers, previously shown to be excellent photocatalysts for H_2 production[16] for CO_2 reduction using $[Co(bpy)_n]^{2+}$ as co-catalyst. This has led to us achieving a five-fold increase in the CO evolution rate. Given that urea derived g-C_3N_4 with a high sp^2:sp^3 N ratio appears to be generally extremely active for photochemical reductions it is important that the factors controlling activity are resolved. Our TA and emission studies show that an increased driving force for charge transfer to a co-catalyst (in this case $[Co(bpy)_n]^{2+}$) or to a sacrificial electron donor is a significant factor. Perhaps surprisingly we also find that the high activity of the urea derived materials correlates with a lower yield of long-lived deeply trapped photogenerated charges, highlighting the importance of defect and other potential charge trap sites in controlling the photochemistry of g-C_3N_4.

Notes and references

JJW and AJC acknowledge the EPSRC (EP/K006851/1) for a funding and a fellowship respectively and for equipment funding (EP/K031511/1). Thanks to Prof. Dave J. Adams and Prof. Dmitry Shchukin (UoL) for providing access to the fluorimeter and FTIR spectrometer, respectively. Thanks to Mr. Mark Forster (UoL) for his help with DR-TA experiments.

1 S. J. A. Moniz, S. A. Shevlin, D. J. Martin, Z.-X. Guo and J. Tang, *Energy Environ. Sci.*, 2015, **8**, 731–759
2 X. Wang, K. Maeda, A. Thomas, K. Takanabe, G. Xin, J. M. Carlsson, K. Domen and M. Antonietti, *Nat. Mater.*, 2009, **8**, 76–80.
3 J. Liu, Y. Liu, N. Liu, Y. Han, X. Zhang, H. Huang, Y. Lifshitz, S. Lee, J. Zhong and Z. Kang, Science, 2015, **347**, 970–974.
4 J. Hong, S. Yin, Y. Pan, J. Han, T. Zhou and R. Xu, *Nanoscale*, 2014, **6**, 14984–14990.
5 L. Shi, L. Liang, F. Wang, M. Liu, K. Chen, K. Sun, N. Zhang and J. Sun, *ACS Sustain. Chem. Eng.*, 2015, **3**, 3412–3419.
6 S. Min and G. Lu, *J. Phys. Chem. C*, 2012, **116**, 19644–19652.
7 X. Zhang, L. Yu, C. Zhuang, T. Peng, R. Li and X. Li, *ACS Catal.*, 2014, **4**, 162–170.
8 Y. Shiraishi, Y. Kofuji, S. Kanazawa, H. Sakamoto, S. Ichikawa, S. Tanaka and T. Hirai, *Chem. Commun.*, 2014, **50**, 15255–15258.
9 C. A. Caputo, M. A. Gross, V. W. Lau, C. Cavazza, B. V Lotsch and E. Reisner, *Angew. Chem. Int. Ed*., 2014, **53**, 11538–11542.
10 X. Wang, G. Zhang, S. Zang, Z. Lan, C. Huang and G. Li, *J. Mater. Chem. A*, 2015, **3**, 17946–17950.
11 G. Dong, Y. Zhang, Q. Pan and J. Qiu, *J. Photochem. Photobiol. C Photochem. Rev.*, 2014, **20**, 33–50.
12 A. Thomas, A. Fischer, F. Goettmann, M. Antonietti, J.-O. Müller, R. Schlögl and J. M. Carlsson, *J. Mater. Chem.*, 2008, **18**, 4893–4908.
13 S. W. Hu, L. W. Yang, Y. Tian, X. L. Wei, J. W. Ding, J. X. Zhong and P. K. Chu, *Appl. Catal. B Environ.*, 2015, **163**, 611–622.
14 K. Takanabe, K. Kamata, X. Wang, M. Antonietti, J. Kubota and K. Domen, *Phys. Chem. Chem. Phys.*, 2010, **12**, 13020–13025.
15 D. J. Martin, P. J. T. Reardon, S. J. a Moniz and J. Tang, *J. Am. Chem. Soc.*, 2014, **136**, 12568–12571.
16 D. J. Martin, K. Qiu, S. A. Shevlin, A. D. Handoko, X. Chen, Z. Guo and J. Tang, *Angew. Chem. Int. Ed.*, 2014, **53**, 9240–9245.
17 Y. Zheng, L. Lin, X. Ye, F. Guo and X. Wang, *Angew. Chem. Int. Ed.*, 2014, **53**, 11926–11930.
18 J. Lin, Z. Pan and X. Wang, *ACS Sustain. Chem. Eng.*, 2014, **2**, 353–358.
19 J. Lin, Y. Hou, Y. Zheng and X. Wang, *Chem. Asian J.*, 2014, **9**, 2468–2474.
20 K. Maeda, K. Sekizawa and O. Ishitani, *Chem. Commun.*., 2013, **49**, 10127–10129.
21 R. Kuriki, K. Sekizawa, O. Ishitani and K. Maeda, *Angew. Chem. Int. Ed.*, 2015, **54**, 2406–2409.
22 R. Kuriki, H. Matsunaga, T. Nakashima, K. Wada, A. Yamakata, O. Ishitani and K. Maeda, *J. Am. Chem. Soc.*, 2016, **138**, 5159–5170.
23 J.-M. Lehn and R. Ziessel, *Proc. Natl. Acad. Sci. USA*, 1982, **79**, 701–704.
24 R. Ziessel, J. Hawecker and J.-M. Lehn, *Helv. Chim. Acta*, 1986, **69**, 1065–1084.
25 J. Grodkowski and P. Neta, *J. Phys. Chem.*, 2000, **104**, 1848–1853.
26 H. Kisch and D. Bahnemann, *J. Phys. Chem. Lett.*, 2015, **6**, 1907–1910.
27 S. Sato, T. Morikawa, S. Saeki, T. Kajino and T. Motohiro, *Angew. Chem. Int. Ed*., 2010, **49**, 5101–5105.
28 E. Pastor, F. M. Pesci, A. Reynal, A. D. Handoko, M. Guo, X. An, A. J. Cowan, D. R. Klug, J. R. Durrant and J. Tang, *Phys. Chem. Chem. Phys.*, 2014, **16**, 5922–5926.
29 J. R. Lakowicz, *Principles of Fluorescence Spectroscopy*, 3rd ed., 2006, p. 289.
30 A. J. Cowan, W. Leng, P. R. F. Barnes, D. R. Klug and J. R. Durrant, *Phys. Chem. Chem. Phys.*, 2013, **15**, 8772–8778.
31 C. Ye, J. X. Li, Z. J. Li, X. B. Li, X. B. Fan, L. P. Zhang, B. Chen, C. H. Tung and L. Z. Wu, *ACS Catal.*, 2015, **5**, 6973–6979.
32 H. Zhang, Y. Chen, R. Lu, R. Li and A. Yu, *Phys. Chem. Chem. Phys.*, 2016, **18**, 14904–14910.
33 H. Kasap, C. A. Caputo, B. C. M. Martindale, R. Godin, V. W.-H. Lau, B. V. Lotsch, J. R. Durrant and E. Reisner, *J. Am. Chem. Soc.*, 2016, **138**, 9183–9192.
34 A. J. Cowan, J. Tang, W. Leng, J. R. Durrant and D. R. Klug, *J. Phys. Chem. C*, 2010, **114**, 4208–4214.
35 A. J. Cowan and J. R. Durrant, *Chem. Soc. Rev.*, 2013, **42**, 2281–2293.
36 W. Wei and T. Jacob, *Phys. Rev. B*, 2013, **87**, 085202.

Photochemical CO_2 reduction using structurally controlled g-C_3N_4

James J. Walsh,[a] Chaoran Jiang,[b] Junwang Tang[b] and Alexander J. Cowan[a]*

[a.] *Stephenson Institute for Renewable Energy, University of Liverpool, L69 7ZF, Liverpool, UK. Email: a.j.cowan@liv.ac.uk*
[b.] *Solar Energy Group, Department of Chemical Engineering, University College London, Torrington Place, London, WC1E 7JE, UK.*

Electronic supplementary information

1 Experimental

Synthesis and materials: The three types of g-C_3N_4 were synthesised according to our previously published method.[S1] g-C_3N_4 was synthesised by thermal condensation of different organic precursors (urea, thiourea and dicyandiamide (DCDA)). Typically, a lidded alumina crucible with half the volume occupied by the precursor was placed inside a muffle furnace and heated at 600°C with a ramp rate of 5°C/min for 4 hours. The resultant powders were washed with deionised water and dried in air at 70°C for several hours before use.

CH_3CN (spec grade, Aldrich), triethanolamine (TEOA, Aldrich), 2,2'-bipyridine (bpy, Aldrich) and $CoCl_2.6H_2O$ (Aldrich) were used as purchased. Milli-Q water was used in all experiments. CO_2 (BOC) was CP grade.

Methods: The reaction suspension (consisting of g-C_3N_4 in 3:1:1 CH_3CN/H_2O/TEOA) was made up in a glass vial and sonicated for 10 minutes to ensure dispersion of the solid g-C_3N_4. The reactor used for photocatalysis was a 1 x 2 cm quartz cuvette (Starna) equipped with a B24 neck adaptor. The reaction suspension was added to this flask with a magnetic stirring bar neck was sealed with a rubber septum and purged with CO_2 for 20 minutes. The reaction mixture containing aqueous-soluble Co^{2+} and organic-soluble bpy phases was stirred vigorously throughout the experiment to prevent phase separation.[S2, S3] Samples for gas chromatography were taken at time zero and at intervals of one hour thereafter.

External quantum yield (EQE) measurements were conducted under LED or monochromated lamp illumination measured for each individual experiment. Optimisation of photocatalytic activity was performed using a 150 W Xe lamp equipped with a KG1 filter under constant power irradiation. Control experiments under argon, in the dark, and in the absence of either g-C_3N_4, TEOA, Co^{2+} or bpy showed minimal or no CO evolution (Table 1). Wavelength-dependent photocatalysis was conducted using a series of LEDs from LEDEngin purchased from RS Electronics: LZ1-00U600 (365 nm), LZ4-00UA00 (400 nm) LED or LZ1-00B200 (465 nm). The 420 nm LED (EPILED) were purchased from Amazon. Each LED was mounted onto a heat sink and driven using banana plugs and a power supply (TTI).

Gas product yields (dihydrogen and carbon monoxide) were quantified using an Agilent 6890N gas chromatograph employing N6 helium as the carrier gas (5 ml.min^{-1}). A 5 Å molecular sieve column (ValcoPLOT, 30 m length, 0.53 mm ID) and a pulsed discharge detector (D-3-I-HP, Valco Vici) were employed. CO and H_2 peak areas were quantified with multiple calibrant gas injections and were re-calibrated daily. ^{1}H-NMR spectroscopy of the post-reaction solution, to test for liquid CO_2 reduction products such as formic acid, was not possible due to the presence of paramagnetic Co^{2+}.

Inductively-coupled plasma mass spectrometry (ICP-MS) was performed using a dissolved g-C_3N_4 colloidal sol.[S4] Three photocatalytic experiments were setup using 365 nm LED at 5 mW/cm^2 for 2 hours. After the reaction, the solid g-C_3N_4 was centrifuged and washed with Milli-Q water. This process was repeated a further two times using clean water. The solid g-C_3N_4 (2.5 mg) was then dissolved in 5 ml of concentrated HNO_3 and refluxed at 80°C for 3 hours. After approximately one hour the cloudy suspension turned clear. The slightly yellow colloidal solution was cooled to room temperature and was stable over a period of several months, with no obvious precipitation. The UV/Vis spectra of the colloids revealed a delaminated solution and correlated well with the literature.[S4] Three post-reaction colloidal solutions were examined for Co content and the averaged data showed good reproducibility.

UV/Vis diffuse reflectance spectroscopy was performed using a Shimadzu 2600 spectrometer equipped with an integrating sphere using either 1 cm quartz cuvettes (suspensions) or glass microscope slides (solids).

Steady-state luminescence measurements were collected using a Perkin Elmer Fluorescence Spectrometer LS55 with slit widths of 10 nm and 2.5 nm at a scan rate of 500 nm/min. Spectra were recorded using suspensions of g-C_3N_4 in 1 x 1 cm

quartz cuvettes fitted with a B24 neck (Starna) and rubber septa. Samples were made by weighing out 1.0 mg g-C_3N_4 into 5 ml H_2O followed by 30 minutes sonication. The samples were then diluted 1:1 with CH_3CN containing bpy to give a final suspension of 0.1 mg/ml g-C_3N_4. Small aliquots (5-25 µl) of a concentrated (mM) Co^{2+} aqueous stock solution were titrated into the cuvette and the sample was purged with N_2 for 20 minutes before recording the spectrum. The excitation wavelength was chosen for each g-C_3N_4 type at a wavelength independent of absorbance changes upon addition of Co^{2+}.

Time-resolved luminescence measurements were recorded using a modified transient absorption setup employing the third harmonic of a Q-switched Nd:YAG laser (Continuum Minilite). Samples of g-C_3N_4 were compressed into solid discs for reflectance measurements using a die press either alone (DCDA, thiourea) or by mixing with an inert additive (urea, which did not form quality pellets without adding an additive such as NaCl). The samples were placed into a 1 x 2 cm quartz cuvette (Starna) fitted with a B24 neck, stoppered and purged with Ar for 20 minutes prior to excitation. The instrument response function (IRF) was recorded using $BaSO_4$. The time response was recorded using 355 nm laser excitation at 0.4 Hz and averaged over 500 shots. The reflected signal was focused through a monochromator and a bandpass filter (455 nm) to the detector. Data were recorded using a Si photodiode and preamplifier (MCA-200Hz) coupled to an oscilloscope (Tektronix TDS 2014C 100 MHz) and a computer running LabVIEW 2011, and were analysed using the deconvolution functions in Decayfit v 1.3 (Fluortools).

Transient absorption spectra were recorded using a diffuse reflectance sampling mode. Briefly, part of the output from a 75 W Xe lamp (OBB/PTi) was focused through a ND 50 % filter and onto the powdered sample held in a 1 mm quartz cuvette. All samples were thoroughly purged with argon (20 minutes) prior to use. The size of the probe beam was *ca.* 5 mm ∅ at the sample. Diffusely scattered light was collected using 1" plano-convex lens (Thor labs, UV grade silica) and directed through a monochromator (OBB/PTi) and a photodiode (Hamamatsu) coupled to a home-made preamplifier. The time resolution of the system (*ca.* 5 µs) was determined by the photodiode response and the amplification stages employed. Samples were excited using a Nd:YAG laser (Continuum Minilite) at 3 Hz, 355 nm, *ca.* 6 ns. The laser pulse was passed through a UV grade diffuser (Thor labs) to ensure that the entire sample is excited by the laser pulse. Experimental data were averaged for typically 100-250 laser shots. The transient data are presented in the manner previously employed in diffuse reflectance TA spectroscopy by Furube *et al.*, where % absorption = (1 - R/R_0) x 100 where R and R_0 are the probe light intensities with and without excitation respectively.[S5] Wavelength-dependent transient data were acquired by adjusting the monochromator settings and recording an averaged kinetic trace every 50 nm.

FTIR spectra were collected using a Bruker Vertex spectrometer operating in transmittance mode. FTIR analysis of isotopically labelled products was performed using a custom built FTIR gas cell. The cell was comprised of plastic tube sealed at each end with 2 mm thick CaF_2 windows (Crystran) and Loctite Hysol epoxy resin (3422 A + B). A 1 cm diameter hole was drilled into the top of the cell and sealed with a fresh septum for each experiment, and the edge of the septum was sealed with silicone gel. The cell, which was *ca*. 2 cm in diameter and *ca*. 10 cm in length, was clamped horizontally in the beam path. Spectra were recorded using air as the background, for 128 scans, at a resolution of 0.5 cm^{-1}. Catalysis was performed using a 365 nm LED for 2 hours using $^{13}CO_2$ as the substrate. After the reaction, 5 ml of gas from the cell headspace were injected into our custom made cell and the spectrum acquired.

2 Optimization of photocatalytic conditions

Parameter						CO (µmol.h^{-1}.g^{-1})
g-C_3N_4	Light[a]	CO_2[b]	bpy	Co^{2+}	TEOA[c]	
Urea	✓	✓	✓	✓	✓	460
×	✓	✓	✓	✓	✓	< 0.01
✓	×	✓	✓	✓	✓	< 0.01
✓	✓	×	✓	✓	✓	0.01
✓	✓	✓	×	✓	✓	< 0.01
✓	✓	✓	✓	×	✓	< 0.01
✓	✓	✓	✓	✓	×	< 0.01

Table S1: Control experiments showing that photocatalysis depends on all factors being present. Conditions: 0.5 mg g-C_3N_4 per ml in CH_3CN/TEOA/H_2O (3:1:1), t = 2 h. a: KG1 illumination (see Fig. S3, λ = 300 – 795 nm with % T ≥ 10, 29 mW.cm^{-2}), b: Purged with Ar, c: Solvent mixture was 3:1 CH_3CN/H_2O.

In addition to the types of g-C_3N_4 screened (shown in Table 1, main paper), the ratios of bpy:Co^{2+} and the quantity of g-C_3N_4 per experiment were both tested over a range of values. An optimum ratio of 100 bpy per Co^{2+} was observed, in-line with studies using other types of g-C_3N_4 and *in-situ* formed $[Co(bpy)_n]^{2+}$.[S6]

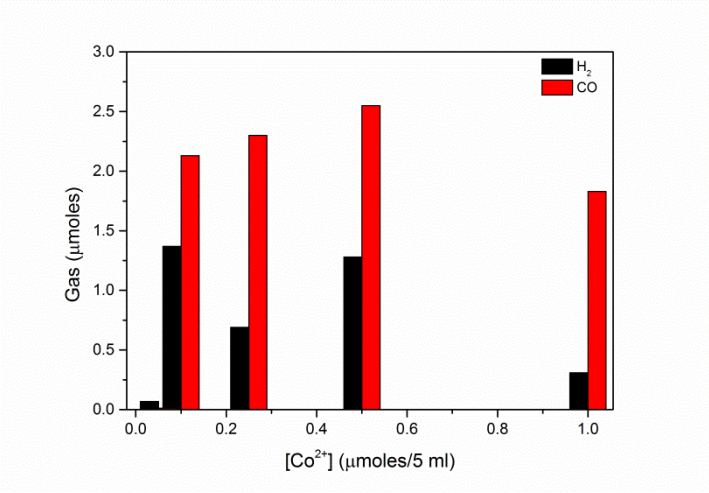

Fig. S1: Varying $[Co^{2+}]$ concentration at constant [bpy] and g-C_3N_4 loading. Conditions: 0.5 mg g-C_3N_4 per ml in $CH_3CN/TEOA/H_2O$ (3:1:1), t = 2 h, under KG1 illumination (see Fig. S3, λ = 300 – 795 nm with % T ≥ 10, 29 mW.cm^{-2}).

The relative photocatalytic efficiencies were then tested using the most efficient type of g-C_3N_4 (urea, data in Table 1) at optimised co-catalyst loading (100:1 bpy/Co^{2+}, data in Fig. S1). This was achieved by changing the loading of suspended g-C_3N_4. These data, shown in Fig. S2, revealed that a g-C_3N_4 concentration 2.5 mg/5 ml yielded the best photocatalytic response. This is likely the g-C_3N_4 loading with an optimum light absorption profile, neither too dilute nor too scattering.

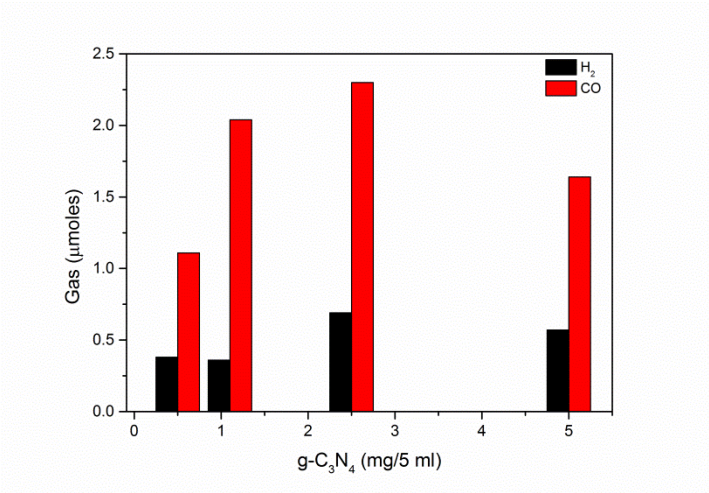

Fig. S2: Comparison of product yields using different quantities of g-C_3N_4 (urea) and constant concentrations of $[Co(bpy)_n]^{2+}$. Conditions: 0.5 mg g-C_3N_4 per ml in $CH_3CN/TEOA/H_2O$ (3:1:1), t = 2 h, under KG1 illumination (see Fig. S3, λ = 300 – 795 nm with % T ≥ 10, 29 mW.cm^{-2}).

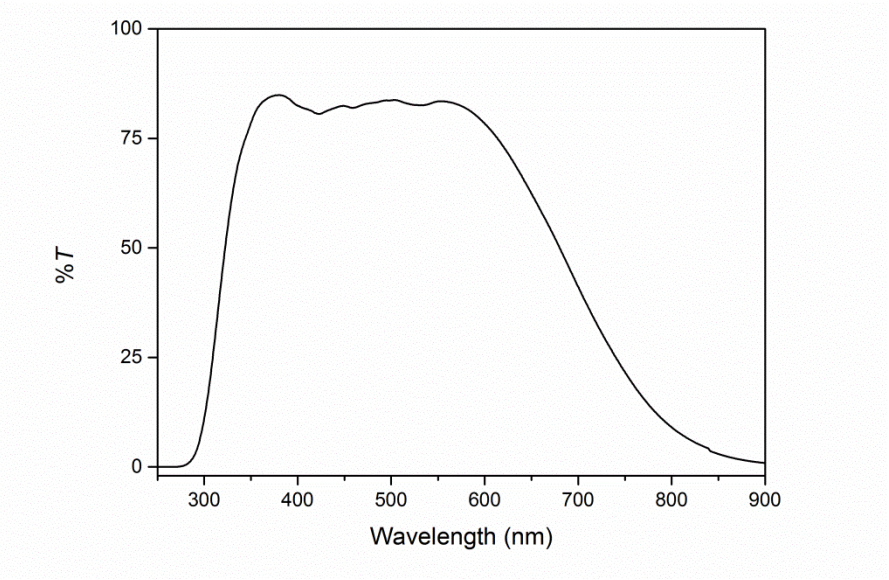

Fig. S3: Transmittance of KG1 filter used in Table 1, Fig. S1 and Fig. S2.

3 LED profiles and AQY measurements

The data in Fig. 1 (b), plotted overlaid with the diffuse-reflectance (DR) UV/Vis spectrum of g-C_3N_4 (urea), show that the photocatalytic activity drops off at 420 nm, in line with the reduced absorptivity of g-C_3N_4 (urea) at this wavelength, and by 465 nm the activity had dropped to zero. The photocatalytic activity is given as apparent quantum yield (% AQY) as calculated using Eq. S1:[S7]

$$\% AQY = \left[\frac{(2.n_{CO}.N_A.h.c)}{(t_{irr}.I.\lambda.A)}\right] 100 \qquad \text{(S1)}$$

Where n_{CO} is moles of CO photogenerated; N_A is Avogadro's constant (6.022 x 10^{23} mol^{-1}); h is Planck's constant (6.626 x 10^{-34} J.s); c is the speed of light (3 x 10^8 $m.s^{-1}$); t_{irr} is the irradiation time; I and λ are the incident intensity ($W.cm^{-2}$) and wavelength of light (nm), respectively; and A is the irradiated area of the cell (cm^2).

4 Spectroscopy

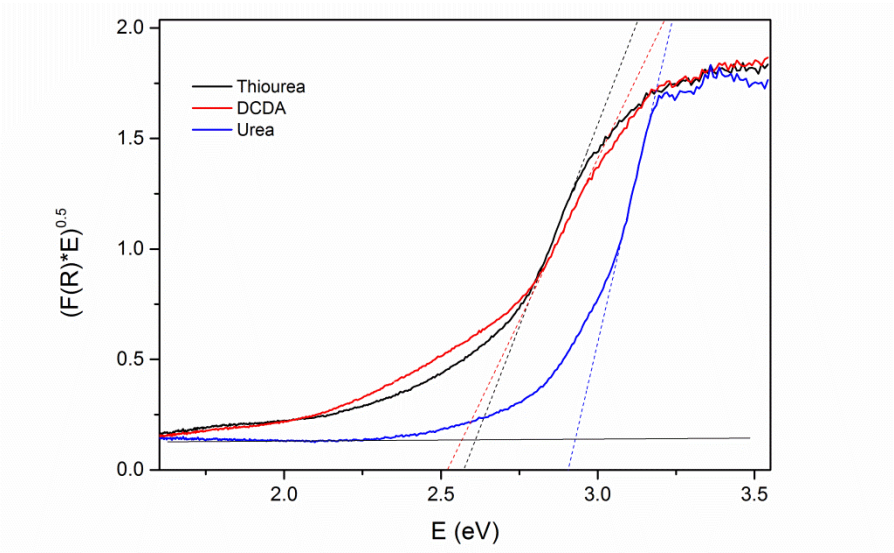

Fig. S4: Tauc plot of g-C_3N_4 derived from the precursors indicted.

Equation	y = a + b*x		
		Value	Standard Error
DCDA	Intercept	1	--
	Slope	17009.58162	63.80002
Urea	Intercept	1	--
	Slope	26252.12814	1275.53042
Thiourea	Intercept	1	--
	Slope	9262.82082	115.37089

Table S2: Fitting data for Stern-Volmer plots in Fig. 2. Data points and error bars are the mean and standard deviation of data from two independent datasets.

The data in Fig. 2 were plotted using the Stern-Volmer equation (Eq. S2):

$$\frac{I_0}{I} = 1 + K_{SV}[Q] \qquad \text{(S2)}$$

Where I and I_0 are the emission intensities of the quenched and unquenched fluorophores, respectively; [Q] is the concentration of Co^{2+} quencher and K_{SV} is the Stern-Volmer constant (Eq. S3):

$$K_{SV} = k_q.\tau_0 \qquad \text{(S3)}$$

From the SV plots it is possible to obtain a quenching rate constant; however care should be taken as the lack of linearity at higher concentrations may indicate the presence of inaccessible emissive sites[S8] and the emission decay kinetics of g-C_3N_4 are also shown to be multi-exponential complicating such analyses. Measurements of the photoluminescent lifetimes using a 355 nm Nd:YAG laser (5-6 ns FWHM) show that the three types of g-C_3N_4 all display lifetimes of similar length and all considerably longer than the IRF (Fig. S5). While the true lifetime values of each g-C_3N_4 type are difficult to measure accurately with our apparatus, we can draw two firm conclusions. Firstly the lifetimes of all three g-C_3N_4 agree very closely, and secondly the lifetimes do not exceed 10 ns. The similarities in τ_0 permit us to estimate relative k_q values for each g-C_3N_4 type, with g-C_3N_4 showing the highest relative k_q. Values for k_q are on the order of 10^{12} s^{-1}, which exceeds the diffusion controlled limit, implying a static quenching mechanism. Indeed, ICP-MS analysis of post-reaction g-C_3N_4 (urea) colloids[S4] revealed the presence of 44 ± 6 ppb Co, in contrast to < 1 ppb for g-C_3N_4 not used in photocatalysis. This corresponds to approximately 3.7 nmol of deposited Co^{2+}, meaning that *ca*. 1.5 molar % of Co^{2+} is deposited throughout a typical reaction (2 hours photocatalysis with 365 nm LED at 5 mW/cm^2). Photodeposition of Co^{2+} onto g-C_3N_4 has been observed previously.[S9, S10] While the photoluminescence experiments were performed under non-catalytic conditions (*i.e.*: in the absence of both CO_2 and TEOA), the ability of Co^{2+} to deposit on g-C_3N_4 can potentially provide a pathway for static quenching and explain the high k_q values obtained. Static quenching has been observed previously for g-C_3N_4 used as a photoluminescent sensor for metallic dications in solution, such as Hg^{2+},[S11] while mixed static/dynamic quenching has been observed for g-C_3N_4 quenching by Cu^{2+}.[S12]

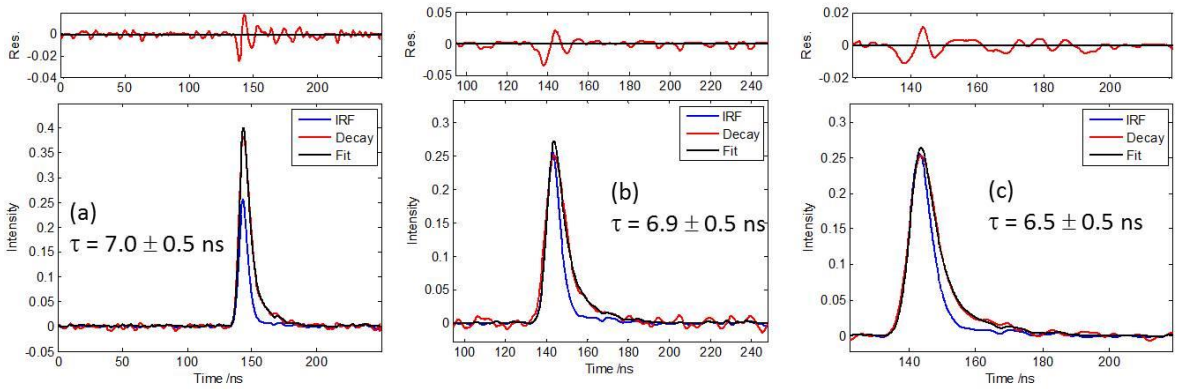

Fig. S5: Time-resolved emission decays monitored at 455 nm following 355 nm excitation of urea (a) thiourea (b) and DCDA (c) derived g-C_3N_4. The IRF is measured using a $BaSO_4$ standard. The lifetimes should be viewed as an approximate value given the similarity between the IRF and the decay functions. Data was fitted using the DecayFit v1.3 software by Fluortools (www.fluortools.com).

Wavelength dependent DR-TA spectra have been normalised for OD response over the range studied.

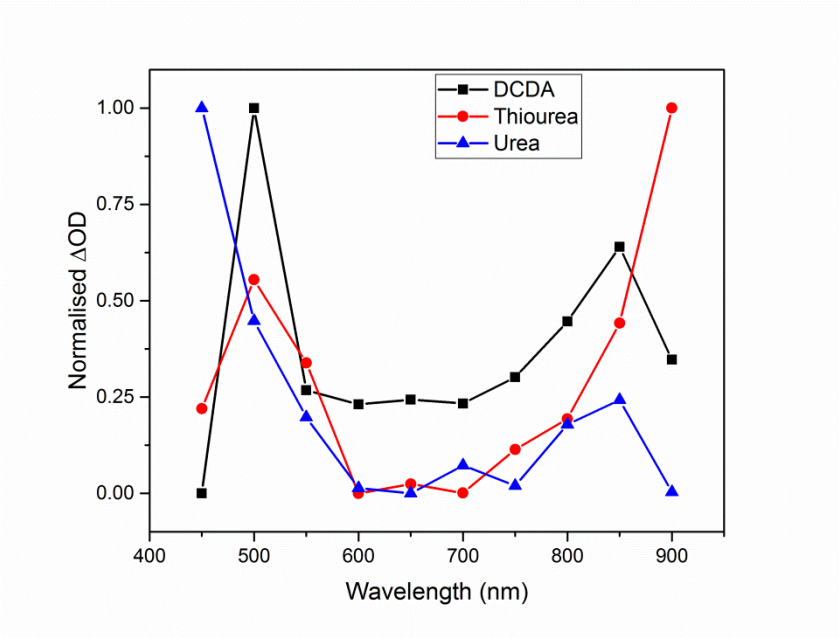

Fig. S6: Diffuse reflectance transient absorption spectra (normalised) 100 µs after laser pulse excitation.

The FTIR spectrum of the products formed from an experiment using $^{13}CO_2$ is shown in Fig. S7. The spectrum shows the presence of the ^{13}CO product with branches centred at 2075 and 2130 cm^{-1}, in line with the literature spectrum for ^{13}CO.[S13] The rising baseline at longer wavelengths is due to the presence of a very large $^{13}CO_2$ absorption. There is no detectable trace of ^{12}CO. The feature centred at 2017 cm^{-1} is due to the $^{13}CO_2$ substrate.

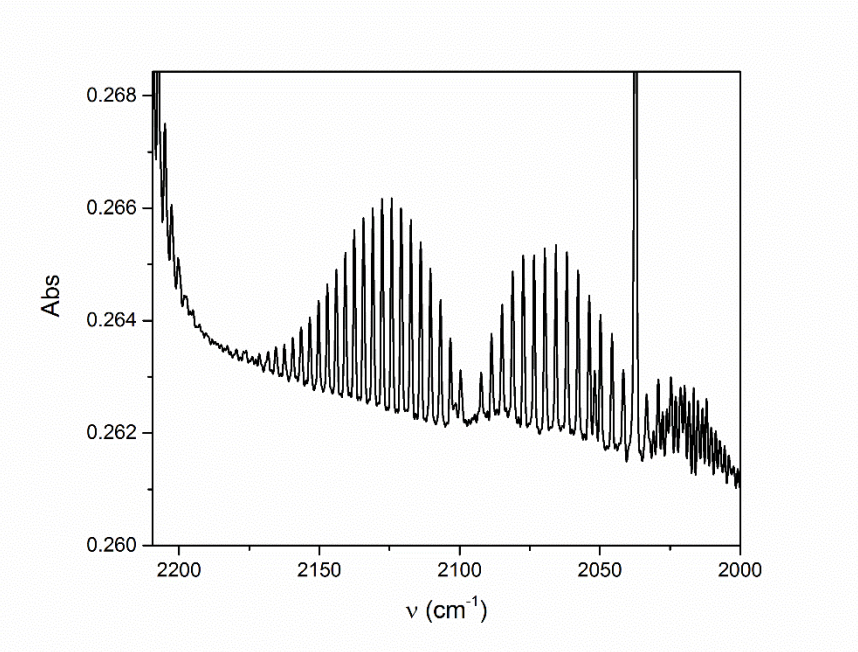

Fig. S7: FTIR spectrum of cell headspace of a $^{13}CO_2$ purged sample post-photocatalysis at 365 nm. The presence of ^{13}CO confirms that CO_2 is the carbon source for the CO production.

5 References

S1 D. J. Martin, K. Qiu, S. A. Shevlin, A. D. Handoko, X. Chen, Z. Guo and J. Tang, *Angew. Chem. Int. Ed.*, 2014, **53**, 9240–9245.

S2 J.-M. Lehn and R. Ziessel, *Proc. Natl. Acad. Sci. USA*, 1982, **79**, 701–704.

S3 R. Ziessel, J. Hawecker and J.-M. Lehn, *Helv. Chim. Acta*, 1986, **69**, 1065–1084.

S4 J. Zhang, M. Zhang, L. Lin and X. Wang, *Angew. Chem. Int. Ed.*, 2015, **54**, 6297–6301.

S5 A. Furube, Z.-S. Wang, K. Sunahara, K. Hara, R. Katoh and M. Tachiya, *J. Am. Chem. Soc.*, 2010, **132**, 6614–6615.

S6 J. Lin, Z. Pan and X. Wang, *ACS Sustain. Chem. Eng.*, 2014, **2**, 353–358.

S7 C. A. Caputo, M. A. Gross, V. W. Lau, C. Cavazza, B. V. Lotsch and E. Reisner, *Angew. Chem. Int. Ed.*, 2014, **53**, 11538–11542.

S8 J. R. Lakowicz, *Principles of Fluorescence Spectroscopy Principles of Fluorescence Spectroscopy*, 3rd ed., 2006, p 289.

S9 R.-L. Lee, P. D. Tran, S. S. Pramana, S. Y. Chiam, Y. Ren, S. Meng, L. H. Wong and J. Barber, *Catal. Sci. Technol.*, 2013, **3**, 1694–1698.

S10 L. Ge, C. Han, X. Xiao and L. Guo, *Appl. Catal. B Environ.*, 2013, **142-143**, 414–422.

S11 S. Barman and M. Sadhukhan, *J. Mater. Chem.*, 2012, **22**, 21832–21837.

S12 N. Cheng, P. Jiang, Q. Liu, J. Tian, A. M. Asiri and X. Sun, *Analyst*, 2014, **139**, 5065–5068.

S13 J. Agarwal, T. W. Shaw, C. J. Stanton, G. F. Majetich, A. B. Bocarsly and H. F. Schaefer, *Angew. Chem. Int. Ed.*, 2014, **53**, 5152–5155.